



# Pleural Line Detection Enhancement in Lung Ultrasonography (LUS) Based on Morphological and Adaptive Structural 2D Filter

Suprijanto<sup>1\*</sup>, Hesty Susanti<sup>2</sup>

<sup>1</sup>Medical Instrumentation Laboratory, Instrumentation and Control Research Group, Faculty of Industrial Technology, Institut Teknologi Bandung, Ganesha 10, Bandung, 40132, INDONESIA

<sup>2</sup>Control, Electronics, and Intelligent Systems (CEIS) Research Group, School of Electrical Engineering, Telkom University, Jalan Telekomunikasi No. 1, Bandung, INDONESIA

\*Corresponding Author

DOI: <https://doi.org/10.30880/ijie.2021.13.05.011>

Received 20 April 2021; Accepted 2 May 2021; Available online 31 July 2021

**Abstract:** Lung ultrasonography (LUS) imaging has been used intensively to investigate and assess the lung's various pathological conditions. A diagnostic system of lung abnormalities is developed to detect and localize the pleural line that can be viewed as the artifacts in LUS image. The continuous pleural line indicates one crucial pattern of a healthy lung. The regular repeated horizontal A-line marks this pattern with a fixed distance between the lines and ideally, produces a higher contrast in the lung image. This work proposes an image processing framework for enhancing pleural line detection in healthy subjects and patients as an early stage of further lung image interpretations in pneumonia patients. The proposed image processing framework is based on a top-hat morphological grayscale 2D filter with a texture structure element and an adaptive structural 2D low pass filter. This framework is evaluated for open dataset video ultrasonography (USG) of Point-of-care ultrasound (POCUS) to enhance the pleural line detection for typical video LUS acquired using a linear and a convex transducer.

**Keywords:** Video Lung Ultrasonography (LUS), pleural line detection, top-hat morphological filter, adaptive low pass filter

## 1. Introduction

Ultrasonography (USG) is a helpful medical imaging modality for investigating the human body's soft tissue anatomically. The advantages of USG are well known, such as its cost-effectiveness, portability, non-invasiveness, and safety better than X-ray imaging. Current studies suggest that Point-of-care ultrasound (POCUS) for lung imaging has significant potential as a diagnostic modality for pathological lung due to COVID-19 [1-7]. POCUS can be used to scan a patient's body directly (bedside). Its imaging device can be transported to wherever the patient is located without a specific scanning room [8], and the image can be interpreted directly on the spot. The application of POCUS can reduce the risk of the infection's spreading.

In the current situation, due to COVID-19 pandemic, the bedside/visual interpretation of lung ultrasonography (LUS) to assess pathological conditions of the lung could be overwhelming for clinicians. In this case, an image processing procedure to enhance the visibility of the main feature on the LUS image becomes a vital necessity to help speed the diagnostic time and increase the accuracy.

Lung ultrasonography (LUS) image interpretation for the diagnostic of lung abnormalities is based on the appearance of specific image artifacts. Evaluation of pleural lines is one of the vital aspects of LUS imaging. Generally, the average

\*Corresponding author: [supri@tf.itb.ac.id](mailto:supri@tf.itb.ac.id)

healthy lung can be characterized by the continuous pleural line (A-line) and the regular repeated horizontal A-line with a fixed distance between the lines. These A-lines are generated by a reverberation or multiple reflections from the pleura with “air space” underneath it. On the contrary, the abnormal lung can be characterized by the discontinuous pleural line and the A-line pattern’s irregularities because of a specific condition, e.g., thickening of A-line due to a fluid present in the *subpleural interlobular septum*. In more severe cases, vertical comet tail artifacts (B-lines) appear under the A-line due to intense multiple reflections from the elements with a large gradient of acoustic impedance around or underneath the pleura, e.g., fluid-rich structures and air-space in *subpleural interlobular septum* and alveoli. A healthy lung correlates with a reflecting pleural line and ideally produces a higher intensity of the pleural line [9-12].

This work focuses on developing an image processing framework for pleural line detection enhancement in LUS image as an early stage of further lung image interpretations in pneumonia patients. The proposed scheme is based on a top-hat morphological grayscale filter with a texture structure element. The adaptive structural low pass filter considering local shape parameters is used to suppress noise and keep the curve line information related to the pleural line.

## 2. Methodology

### 2.1 Image Processing for Pleural Line Detection

Usually, LUS imaging is performed to acquire lung anatomy that represents in time series of image. In LUS, several factors must be considered to optimize the image quality. The setting of imaging parameters in USG machines (i.e., power of US wave, bandwidth and central frequency of the pulse, setting of time gain compensation (TGC) to optimize contrast), and type of transducer (i.e., convex or linear and frequency bandwidth transducer) is correlated with image quality.

On a healthy lung, a surface of the pleural and lung cavity is an almost perfect reflector. It generates horizontal line artifacts and appears as multiple A-lines due to reverberations between the probe and the pleural line [10,18]. Some image processing schemes have been proposed for pleural line detection. In [11,12], contrast enhancement and morphological filtering with the flat structuring elements method were proposed for the pleural line detection. A method based on spatial filtering, segmentation, and machine learning was reported in [13]. Another technique for pleural line detection is proposed by Carrer, L., et al. [10] using a circular averaging filtering and the Viterbi algorithm. The Radon transform was also proposed to identify the pleural line by searching for the brightest horizontal line [19,20].

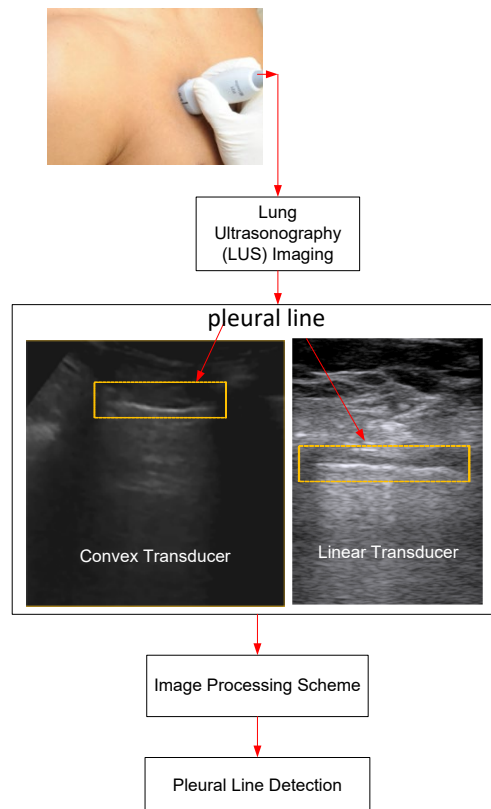


**Fig. 1 - General framework concept of pleural line detection**

The general framework proposed in this work is shown in Fig. 1. On the image processing scheme, two image processing steps are performed, i.e. (1). top-hat morphological grayscale 2D-filter with a texture structure element and (2). adaptive structural 2D low pass filter. Further description of the proposed processing framework concept is explained in the next section.

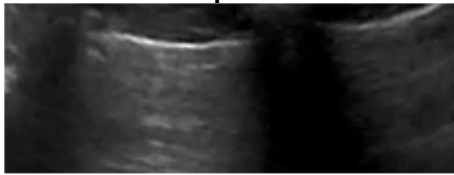
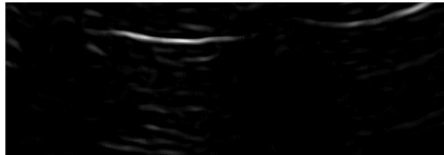
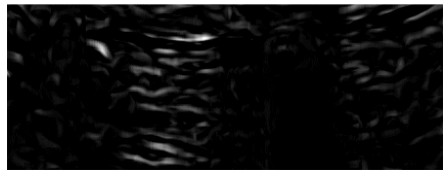
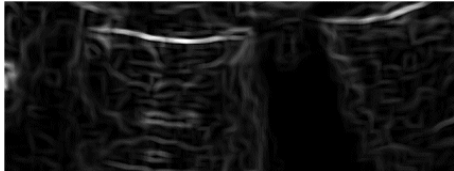
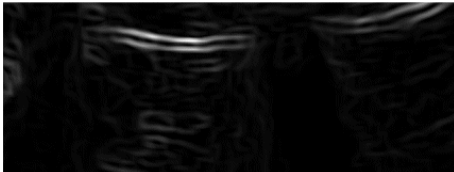
## 2.2 Gray Scale Morphological Filter

The top-hat grayscale morphological filter is an operation to extract a pleural line from an undesired background [15,16] using an operator for closing or opening the morphology of the image. Given  $A(x,y)$  and  $B(j,k)$  describe the gray-level of LUS image and the structural element matrix respectively, the definition of grayscale opening and grayscale closing [21] are:

$$\text{Opening: } O_G(A,B) = D_G(E_G(A,B),B) \quad (1)$$

$$\text{Closing: } C_G(A,B) = E_G(D_G(A,B),B) \quad (2)$$

**Table 1 - Type of top-hat grayscale morphological filter and examples of the results for pleural line detection enhancement in LUS grayscale image**

Type of top-hat filter (THF)	Operator formulation	$A(x,y)$ represents LUS grayscale image with the pleural line 
THF white texture (THF-WT) with size $B(j,k)$ is $13 \times 13$	$A_{ht} = A - O_G(A,B)$	$A_{ht}$ 
THF black texture (THF-BT) with size $B(j,k)$ is $13 \times 13$	$A_{ht} = C_G(A,B) - A$	$A_{ht}$ 
THF white object (THF-WO) with size $B(j,k)$ is $13 \times 13$	$A_{ht} = O_G(A,B) - E_G(A,B)$	$A_{ht}$ 
THF black object (THF-BO) with size $B(j,k)$ is $13 \times 13$	$A_{ht} = O_G(A,B) - C_G(A,B)$	$A_{ht}$ 

Where  $D_G$  and  $E_G$  represent grayscale dilatation and erosion operation, respectively. Grayscale dilation  $D_G(.)$  and grayscale erosion  $E_G(.)$  are given as:

$$D_G(A, B) = \max_{[j,k] \in B} \{A[x - j, y - k] + b[j, k]\} \quad (3)$$

$$E_G(A, B) = \min_{[j,k] \in B} \{A[x - j, y - k] + b[j, k]\} \quad (4)$$

The four types of top-hat grayscale morphological filters and the examples of THT-WT, THT-BT, THF-WO, and THF-BO applications in the images are summarized in Table 1. The subtraction between the LUS grayscale image with the opening operation is a candidate for image processing on the following steps.

### 2.3 Adaptive Structural 2D Low Pass Filter

The output of the processing step in the top-hat filter ( $A_{ht}$ ) is still required further processing. The conventional low pass filtering (LPF) reduce noise by assuming that the signal at some point changes slowly compared to the noise that formulated as:

$$Ao(m, n) = \sum_{j=-h}^{j=h} \sum_{k=-w}^{k=w} f(x - j, y - k) A_{ht}(j, k) \quad (5)$$

The size of the windows filter  $f(\cdot)$  is  $2w + 1$  and  $2h + 1$ , respectively. For LPF with the Gaussian filter, the kernel filter size and variance ( $\sigma$ ) determine the output of filtering image  $Ao(\cdot)$ . The Gaussian LPF can reduce background noise by assuming the desired image and the noise are spectrally separable. In the LUS image, this is only partly true due to noise from the lung region with low acoustic impedance, such as an air region.

In this case, a scheme called adaptive filter is proposed. The main idea of the adaptive filter is applying local adapting to the shape of the filter windows. The parameters related to the structure of the LUS image are included as parameters in the adaptive filter [14]. The structural parameters are based on scale and orientation. The idea of adaptive filtering is depicted in Fig. 2.

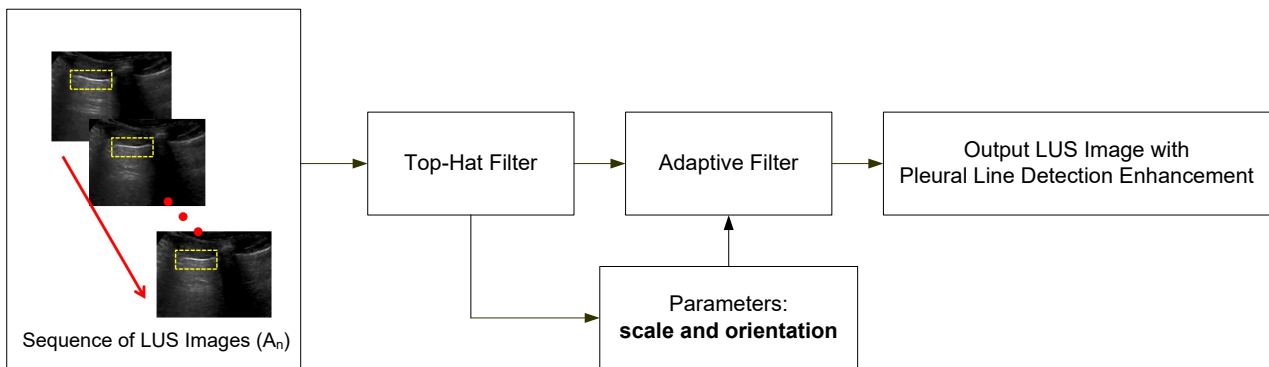


**Fig. 2 - The concept of adaptive filtering**

The parameters of orientation and curvature are derived using gradient structure tensor (GST). The basic of GST consists of these following steps:

Step 1: Estimating the gradient of  $g = \nabla A_{ht}$  at scale  $\sigma_g$ . The  $A_{ht}$  convolving with the first-order derivative of a Gaussian  $G(\cdot)$ . For two dimensional image, the component gradient is:

$$g_i = A(X) * \frac{\partial}{\partial x} G(X; \sigma_g), X = \{x, y\} \quad (6)$$

Step 2: The mapping of GST using the dyadic product and averaging the tensor component  $T_{ij}$  at scale  $\sigma_T$ . The GST defined by:

$$T \equiv \overline{gg^T} \quad (7)$$

The elements of the GST can be viewed as gradient energies. In the computation of local average or spatial integration, the tensor component is convolving with a Gaussian kernel  $G(\cdot)$  that is defined as:

$$\overline{T}_X = T_X * G(X; \sigma_T), X = \{x, y\} \quad (8)$$

In the computation of local average or spatial integration, the tensor component is convolving with a Gaussian kernel. The tensor scale is usually chosen three to ten times the gradient scale:  $3 \sigma_g < \sigma_T < 10\sigma_g$ .

The advantage of averaging the tensor is that the rapid change in the orientation due to noise on the gradient image can be suppressed, resulting in a smooth orientation estimate. With the proper chosen value of  $\sigma_g$  and  $\sigma_T$ , a small discontinuous line may be smoothed while still keeping the main structure of the line. In Fig. 3, the filtering process of  $I_{ht}$  (THF-WT) based is shown. The comparing results from the conventional LPF filter ( $\sigma = 2$ ) and adaptive filter ( $\sigma_g = 2$  and  $\sigma_T = 5$ ) are illustrated in Fig. 3.

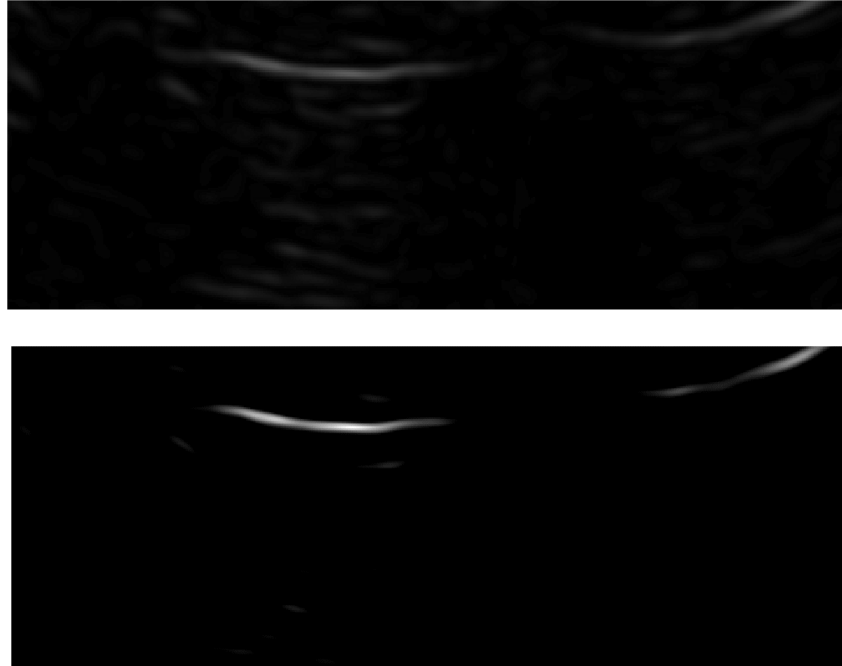


**Fig. 3 - Comparison results from (top) conventional LPF filter ( $\sigma = 2$ ); and (bottom) adaptive filter ( $\sigma_g = 1$  and  $\sigma_T = 5$ ) with LUS image shown in Table 1**

### 3. Results and Discussion

#### 3.1 Results for the Convex Transducer

The open data set of video LUS [17] was used to evaluate our image processing framework. The data set A and B were acquired using a convex transducer with a frame rate of about 50 fps, resolution  $852 \times 852$ , and the frame length in about  $n = 50$  frames. The parameters of processing steps are tabulated in Table 2.

**Table 2 - Processing parameters for the convex transducer**

Data set	THF-WT parameters	Adaptive filtering
A	Windows shape: rectangular with size $13 \times 13$	$\sigma_g = 1$ and $\sigma_T = 5$
B	Windows shape: rectangular with size $17 \times 17$	$\sigma_g = 1$ and $\sigma_T = 10$

The results from data set A and B are illustrated in Fig. 4 and Fig. 5, respectively. Using only THF-WT, the pleural lines in 4 different frames are shown. The remaining background noise and discontinuous lines can be suppressed and corrected using THF-WT and the adaptive filter.

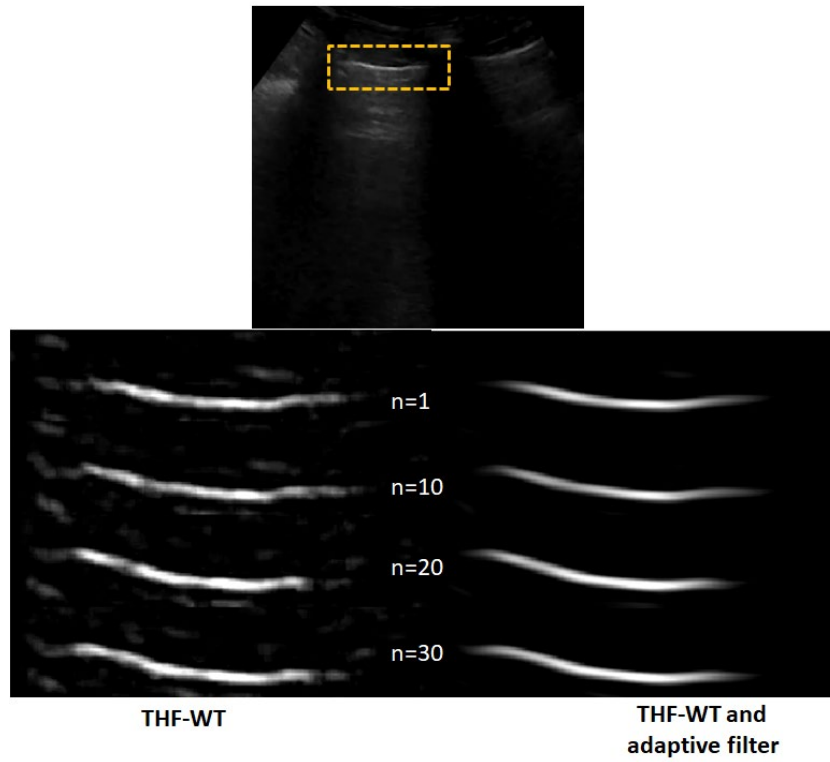


Fig. 4 - The resulting pleural line detection from data set A; the pleural line selected from the region of interest (marked by the yellow box) is detected

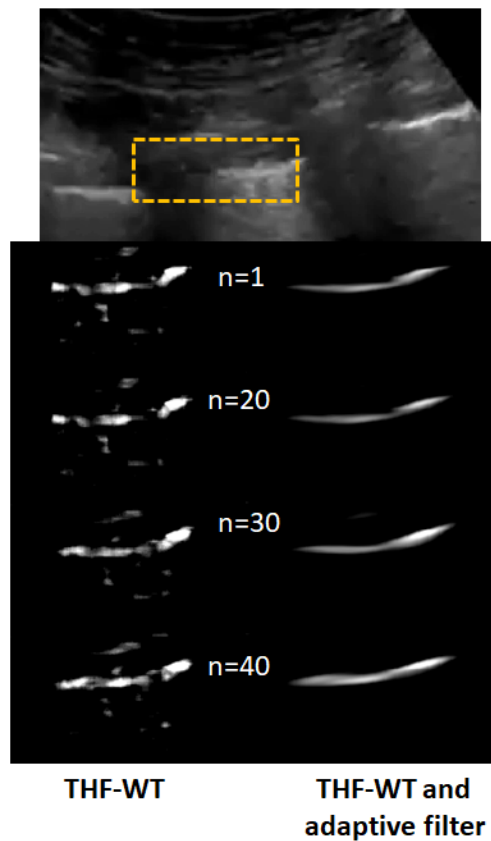


Fig. 5 - The resulting pleural line detection from data set B; the pleural line selected from the region of interest (marked by the yellow box) is detected

### 3.2 Results for the Linear Transducer

The data set C was acquired using a linear transducer with a frame rate of about 30 fps, resolution  $400 \times 400$ , and the frame length in about  $n = 50$  frames. Data set C was obtained from a normal lung [17]. The data set D was acquired using a linear transducer with a frame rate of about 25 fps, resolution  $420 \times 420$ , and the frame length in about  $n = 60$  frames. Data set D was obtained from an abnormal lung [17]. The parameters of processing steps are tabulated in Table 3.

**Table 3 - Processing parameters for the linear transducer**

Data Set	THF-WT parameters	Adaptive filtering
C	Windows shape: rectangular with size $13 \times 13$	$\sigma_g = 1$ and $\sigma_T = 5$
D	Windows shape: rectangular with size $13 \times 13$	$\sigma_g = 1$ and $\sigma_T = 5$

The results from data set C and D are illustrated in Fig. 6 and Fig. 7. Using only THF-WT, the pleural lines in 3 different frames are shown. The remaining background noise and discontinuous lines can be suppressed and corrected using THF-WT and adaptive filter. The discontinuity of the pleural lines from data D is clearly shown in Fig. 7.

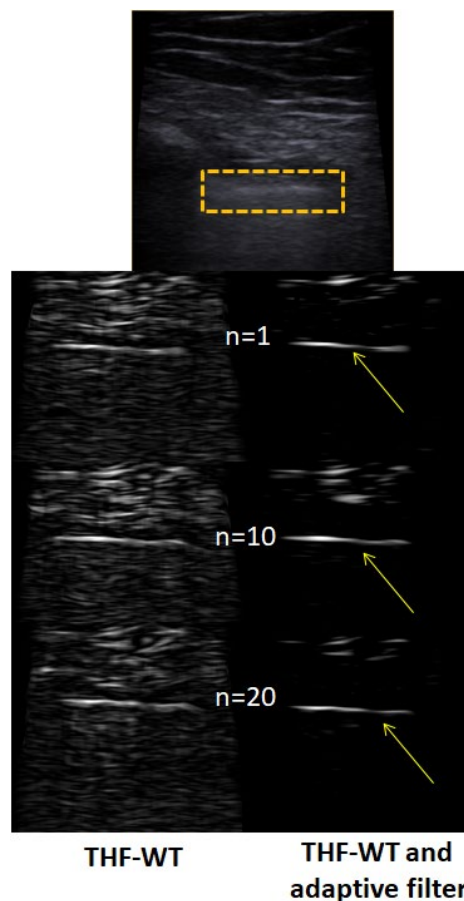


**Fig. 6 - The resulting pleural line detection from data set C; the pleural line selected from the region of interest (marked by the yellow box) is detected**

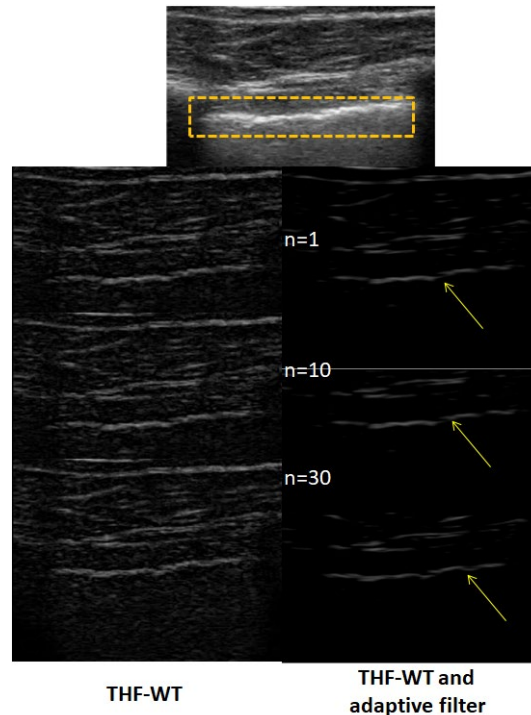


**Fig. 7 - The resulting pleural line detection from data set D; the pleural line selected from the region of interest (marked by the yellow box) is detected; the discontinuity of the pleural line is detected using THF-WT and the adaptive filter**

### 3.3 Discussion

The alternative image processing framework to support pleural line detection in the LUS is proposed. The proposed scheme is based on a top-hat morphological grayscale 2D filter with a texture structure element and followed with an adaptive structural 2D low pass filter. This framework is evaluated for open dataset video USG of POCUS.

The proposed scheme is succeeded in enhancing pleural line detection in healthy subjects and patients. It is intended as an early stage of further lung image interpretations in pneumonia patients for typical video LUS acquired using a linear and a convex transducer. In future work, the proposed scheme can be used as a part of feature extraction techniques to support automatic pleural line detection using machine learning to enhance reliability classification of lung abnormality based on LUS image.

### Acknowledgement

We acknowledge the Ministry of Research and Technology of the Republic of Indonesia for competency-based research funding 2020.

### References

- [1] Buonsenso, D., et al. (2020). Point-of-care lung ultrasound findings in novel coronavirus disease-19 pneumoniae: a case report and potential applications during COVID-19 outbreak. *European Review for Medical and Pharmacological Science*, 24(5), 2776-2780.
- [2] Fiala, M. J. (2020). A brief review of lung ultrasonography in COVID-19: is it useful? *Annals of Emergency Medicine*, 75(6), 784-785.
- [3] Poggiali, E., et al. (2020). Can lung US help critical care clinicians in the early diagnosis of novel coronavirus (COVID-19) pneumonia? *Radiology*, 295(3), E6.
- [4] Huang, Y., et al. (2020). A preliminary study on the ultrasonic manifestations of peripulmonary lesions of non-critical novel coronavirus pneumonia (COVID-19). *Research Square*, in press.
- [5] Koenig, S., & Tsegaye, A. (2019). POINT: should point-of-care ultrasound examination be routine practice in the evaluation of the acutely breathless patient? yes. *Chest*, 156(3), 424-426.
- [6] Peng, Q. Y., Wang, X. T., & Zhang, L. N. (2020). Findings of lung ultrasonography of novel corona virus pneumonia during 2019-2020 epidemic. *Intensive Care Medicine*, 46, 849-850.
- [7] Yoo, J., et al. (2020). Emergency department lung ultrasound findings in novel coronavirus. *Annals of Emergency Medicine*, in press.

- [8] Kulkarni, S., Down, B., & Jha, S. (2020). Point-of-care (POC) lung ultrasound in intensive care during the COVID-19 pandemic. *Clinical Radiology*, 75(9), 710.e1-710.e4.
- [9] Lichtenstein, D. A., & Mezière G. A. (2008). Relevance of lung ultrasound in the diagnosis of acute respiratory failure: the BLUE protocol. *Chest*, 134(1), 117-125.
- [10] Carrer, L., et al. (2020). Automatic pleural line extraction and COVID-19 scoring from lung ultrasound data. *IEEE Transactions on Ultrasonics, Ferroelectrics, and Frequency Control*, in press.
- [11] Moshavegh, R., et al. (2016). Novel automatic detection of pleura and B-lines (comet-tail artifacts) on in-vivo lung ultrasound scans. In N. Duric, & B. Heyde (Eds.), *Proceedings of SPIE* (pp. 97900K, vol. 9790).
- [12] Moshavegh, R., Hansen, K. L., Moller-Sorensen, H., Nielsen, M. B., & Jensen, J. A. (2020). Automatic detection of B-lines in vivo lung ultrasound. *IEEE Transactions on Ultrasonics, Ferroelectrics, and Frequency Control*, 66(2), 309-317.
- [13] Correa, M., et al. (2018). Automatic classification of pediatric pneumonia based on lung ultrasound pattern recognition. *PLoS ONE*, 13(12), e0206410.
- [14] Bakker, P. (2002). Image structure analysis for seismic interpretation, Dissertation, TU Delft Netherlands.
- [15] Bright, D., & Steel, E. (2011). Two-dimensional top hat filter for extracting spots and spheres from digital images. *Journal of Microscopy*. 146, 191-200.
- [16] Bai, X., Zhou, F., & Xue, B. (2012). Image enhancement using multi-scale image features extracted by top-hat transform. *Optics and Laser Technology*, 44, 328-336.
- [17] Born, J., et al. (2020). POCOVID-Net: automatic detection of COVID-19 from a new lung ultrasound imaging dataset (POCUS). *ArXiv preprint*, 2004.12084v3, in press.
- [18] McDermott, C., et al. (2021). Sonographic diagnosis of COVID-19: a review of image processing for lung ultrasound. *Frontiers in Big Data*, 4, 612561.
- [19] Anantrasirichai, N., Hayes, W., Allinovi, M., Bull, D., & Achim, A. (2017). Line detection as an inverse problem: application to lung ultrasound imaging. *IEEE Transactions on Medical Imaging*, 36(10), 2045-2056.
- [20] Karakus, O., Anantrasirichai, N., Aguersif, A., Silva, S., Basarab, A., & Achim, A. (2020). Detection of line artifacts in lung ultrasound images of COVID-19 patients via nonconvex regularization. *IEEE Trans Ultrason Ferroelectr Freq Control*.
- [21] Hassanpour, H., Samadiani, N., & Salehi, S. M. M. (2015). Using morphological transforms to enhance the contrast of medical images. *The Egyptian Journal of Radiology and Nuclear Medicine*, 46(2).